Journal of Solid State Chemistry 183 (2010) 2068–2076

Contents lists available at ScienceDirect

Journal of Solid State Chemistry

journal homepage: www.elsevier.com/locate/jssc

Second order incommensurate phase transition in 25L-Ta_2O_5

M. Audier [a,*], B. Chenevier [a], H. Roussel [a], A. Lintanf Salaün [b]

[a] Laboratoire des Matériaux et du Génie Physique, UMR CNRS 5628, Minatec - INP Grenoble, 3 parvis Louis Néel, BP 257, 38016 Grenoble Cedex 1, France
[b] Tyndall National Institute Lee Maltings prospect row, Cork, Ireland

ARTICLE INFO

Article history:
Received 20 May 2010
Received in revised form
2 July 2010
Accepted 3 July 2010
Available online 16 July 2010

Keywords:
L-Ta_2O_5 structures
25L-Ta_2O_5 superstructure
Incommensurate phase transition

ABSTRACT

A new structural state 25L-Ta_2O_5, obtained from sintering and annealing treatments of a Ta_2O_5 powder, is identified both by electron diffraction and high resolution imaging on a transmission electron microscope (TEM). According to general rules for the different L-Ta_2O_5 structures proposed by Grey et al. (J. Solid State Chem. 178 (2005) 3308), a structural model is derived from their crystallographic data on 19L-Ta_2O_5. This model yields simulated images in agreement with high resolution TEM observations of the structure oriented along its [001] zone axis, but only for a very thin crystal thickness of less than 1.2 nm. Such a limitation is shown to be due to a modulation of the structure along its [001] axis. Actually, from an analysis of a diffuse scattering and of its evolution into satellites reflections as a function of the cooling rate, a second order incommensurate phase transition can be assumed to occur in this compound. The property of single phase samples observed by TEM is also verified by X-ray powder diffraction. In a discussion about studies performed by different authors on incommensurate structures in the system Ta_2O_5–WO_3, it is noticed that TEM results, similar to ours, indicate that phase transitions could be expected in these structures.

1. Introduction

Many crystallographic studies have been performed on low temperature Ta_2O_5-type phases since Roth and Stephenson [1] have shown they are based on the UO_3-type structure and form a homologous series of stable phases in the system Ta_2O_5–WO_3 [2–5]. The crystal chemistry of these structures has recently been revisited by Grey et al. [6] with a determination of a new structure, called 19L-Ta_2O_5, using a single crystal sample likely stabilized by the incorporation of a small amount of lithium (0.14 wt% Li). In the notation of structure, L stands for low temperature phase, i.e. for $T \lessapprox 1320$ °C where Ta_2O_5 undergoes a structural transformation [7][1] and 19 is a multiple integer (m) of a parameter b_0 of an orthorhombic sub-cell proposed by Lehovec [8] ($a_0=6.20$ Å, $b_0=3.66$ Å, $c_0=3.89$ Å). The approach of Lehovec has been proved to be very useful since different L-Ta_2O_5 related structures with different multiplicities of 5, 8, 11, 13, 14 and 19 were identified [6] (and references there-in). Grey et al. [6] recall in their article that the m values obey to specific rules. They propose a general model that can explain the structural chemistry in the known m L-Ta_2O_5-related structures but also allows one to predict other structures. All these structures are constituted of similar polyhedra corresponding to TaO_6 octahedra and TaO_7 pentagonal bipyramids which, assembled in different sequences, exhibit a symmetry either C or P. But, since incommensurate structures with wave vectors of modulation along the [010] axis have also been observed in the system Ta_2O_5–WO_3 [9–11], the model of Grey et al. might be considered as describing commensurate lock-in phases as a function of the Ta_2O_5/WO_3 ratio.

In studies related to applications of thin film layers of Ta_2O_5 as high-k materials in electronic devices [12,13], we were interested to derive structures from the model of Grey et al. [6] in order to perform image simulations to be compared to high resolution transmission electron microscopy (HRTEM) images. Actually, if their model has allowed us to find a good agreement between image simulations and observations, curiously it was only for very thin layers of less than 1.2 nm oriented along a [001] zone axis, which was parallel (or almost) to the normal of the layer surface [14]. After many unsuccessful attempts for simulating HRTEM images of thicker layers we were led to assume that this problem might be due to a slightly different stacking of (001) layers of polyhedra in Ta_2O_5. As, to our knowledge, any TEM study has not been published on this aspect, we have performed a study on a Ta_2O_5 powder in order to determine if a modulation does occur along [001] or not. A commercial Ta_2O_5 powder was chosen because high resolution images of different L-Ta_2O_5 structures of [001] zone axis, published by different authors [15,11], exhibit similar features to those we have observed on thin films.

In the present article, we report on a new 25L-Ta_2O_5 structure and of its transformation into an incommensurate phase through

* Corresponding author. Fax: +33 456529301.
E-mail address: Marc.Audier@grenoble-inp.fr (M. Audier).

[1] Such a structural transformation depends probably on the purity of the Ta_2O_5 phase because it has not been observed by Grey et al. [6] in their sample containing a small amount of lithium.

0022-4596/$ - see front matter © 2010 Elsevier Inc. All rights reserved.
doi:10.1016/j.jssc.2010.07.001

annealing treatments. The experimental results (Section 3), obtained by selected area electron diffraction (SAED), HRTEM imaging and X-ray diffraction, are presented in three subsections: In Section 3.1, both *a* and *b* cell parameters of 25L-Ta_2O_5 are identified by SAED and HRTEM imaging. A simulation of a HRTEM image of a very thin sample is based on a 25L-Ta_2O_5 structural model derived from the structural rules and crystallographic data on 19L-Ta_2O_5 of Grey et al. [6]. X-ray powder diffraction diagrams are also compared to a simulated diagram of this 25L-Ta_2O_5 structural model. In Section 3.2, a diffuse scattering located in planes normal to [001] is shown to be structured and characteristic of a superstructure. HRTEM observations of samples cooled down more or less rapidly indicate also a modulation of the structure along its [001] axis. In Section 3.3, a phase transition to an incommensurate modulated phase, characteristic of new Bragg reflections, is shown to occur through a very slow cooling from 1000 °C (0.1 °C min^{-1}). The phase transition is assumed to be of second order from the property of single phase state, observed by TEM and X-ray diffraction after each thermal treatment. Finally, we notice in a discussion (Section 4) that incommensurate phase transitions could probably be observed in the system Ta_2O_5–WO_3, on account of electron diffraction patterns presented by Schmid et al. [10,16].

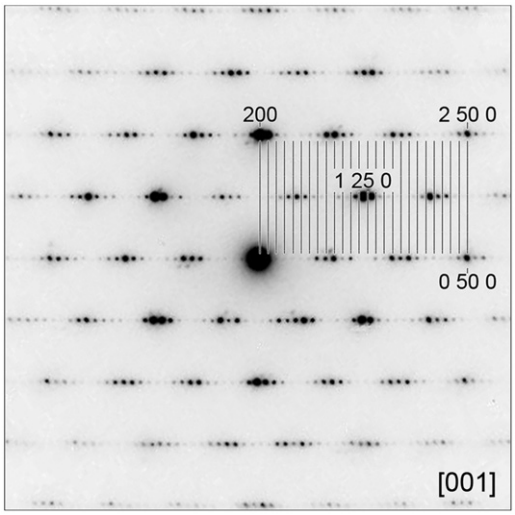

Fig. 1. SAED pattern of [001] zone axis of the Ta_2O_5 sample cooled down at a rate of 5 °C min^{-1} from 1000 °C. Lines drawn on the pattern are an help for verifying the periodicity of the reflections and a C-centering compatible with a monoclinic space group *C*112/*m*. From the indexed reflections corresponding to those of the Lehovec sub-cell, one deduces that $b_0^* = 25b^*$ assuming $a_0^* = a^*$ (see text).

2. Experimental

A commercial Ta_2O_5 powder of 99.9% purity (SIGMA Lot 61H3532) has been used. An iron impurity was identified from an analysis by X-ray energy dispersive spectroscopy. This powder was compressed into a pellet $\varnothing$ 10 mm × 1 mm under a pressure of about 1 GPa and sintered at 1210 °C. The sintered pellet was cooled down within the furnace after switching off the electrical power. Further annealing treatments were successively performed at 1000 ± 10 °C in air for 1 h followed by cooling at different regimes: firstly a rapid cooling by removing the sample from the furnace and then cooling at decreasing rates of 5, 1 and 0.1 °C min^{-1}. TEM observations were carried out on a JEOL 2011 UHR and X-ray powder diffraction diagrams were recorded on a $\theta/2\theta$ goniometer using the Cu Kα1 wavelength. TEM samples were small fragments, obtained by crushing sample pieces in a agate mortar, which were deposited on copper grids coated with holey carbon films.

3. Results

3.1. 25L-Ta_2O_5 structure

Fig. 1 shows a SAED pattern of [001] zone axis of the sample cooled down at a rate of 5 °C min^{-1} from 1000 °C. The set of intense reflections, indexed as 2 0 0, 1 2 5 0, 0 5 0 0 and 2 5 0 0 correspond also to reflections of the C-centered orthorhombic sub-cell of Lehovec, i.e. 2 0 0, 1 1 0, 0 2 0 and 2 2 0, respectively. Thus, for $d_{200} = a_0/2 = 3.10$ Å, one obtains $d_{0\,50\,0} = b_0/2 = 1.83$ Å and a *m* value of 25 such that $b = 25b_0 = 91.5$ Å. Like for the space-group symmetry of 19L-Ta_2O_5, the structure can be assumed to be of monoclinic space group *C*112/*m* with $\gamma \approx 90^\circ$ since the observed *hk*0 reflections satisfy the condition $h+k=2n$ (*n* integer). Let us note that the periodicity along the *b*-axis has also carefully been verified from HRTEM images taken at different magnifications.

Similar SAED patterns of [001] zone axis were observed from different samples, cooled down from 1210 °C, rapidly cooled and cooled down at a rate of 1 °C min^{-1} from 1000 °C. But, as shown after, SAED patterns corresponding to this type of zone axis are slightly different for the sample cooled down at a rate of 0.1 °C min^{-1}.

A structural model of 25L-Ta_2O_5 was required for carrying out image simulations of HRTEM observations. It was determined using structural rules on Ta_2O_5 phases proposed by Grey et al. [6] and their crystallographic data on 19L-Ta_2O_5.

Let us first recall a description of the 19L-Ta_2O_5 structure from which an atomic model of 25L-Ta_2O_5 can be deduced. The structure of 19L-Ta_2O_5 is composed of a stacking of alternating layers of Ta+O atoms at $z=0$ and O atoms at $z=\frac{1}{2}$. A plane of Ta+O atoms normal to [001] is shown in Fig. 2(a) where Ta atoms are represented by large balls of different colors, red, yellow and green and O atoms by small balls of blue color. The *x*,*y* coordinates of O atoms in the plane $z=\frac{1}{2}$ correspond to those of Ta atoms in the plane at $z=0$. Each Ta atom of yellow and red color is surrounded by seven O atoms situated at the vertices of a distorted pentagonal bipyramid; There are five O at $z=0$ and two O at $z=+\frac{1}{2}$ and $-\frac{1}{2}$. Each Ta atom of green color is surrounded by six O atoms at the vertices of a distorted octahedron with four O at $z=0$ and two O at $z=+\frac{1}{2}$ and $-\frac{1}{2}$. The pentagonal bipyramids centered on red and yellow Ta atoms form folded chains of edge shared polyhedra (Fig. 2(a)). Green Ta atoms in octahedral sites are in between these folded chains. Both red and yellow colors of Ta atoms are used in order to emphasize a composite structure constituted of a periodic inter-growth of two structures. Both these structures are assembled by pseudo twin planes parallel to (010). The edge shared chains of TaO_7 bipyramids are a function of this pseudo twinning and correspond to a sequence of straight portions of $n_1=8$ and $n_2=6$ edge shared pentagonal bipyramids. From the relationship between n_1, n_2 and *m* [1], one obtains $m=\frac{3}{2}n_1-1+\frac{3}{2}n_2-1=19$. A rule introduced by Grey et al. [6] is that the chain of edge shared TaO_7 bipyramids must exhibit a "maximum alternation" of chain lengths, that is a sequence 8-6-8-6 rather than 8-8-6-6 as initially proposed by Roth and Stephenson [1]. Therefore, the sequence of the folded chain of edge shared TaO_7 bipyramids must be 8-10-8-10 for the 25L-Ta_2O_5 structure. In this case, atomic coordinates of the 25L-Ta_2O_5 structure could be deduced from those of 19L-Ta_2O_5 through a change of basis and operations of centro-symmetry and

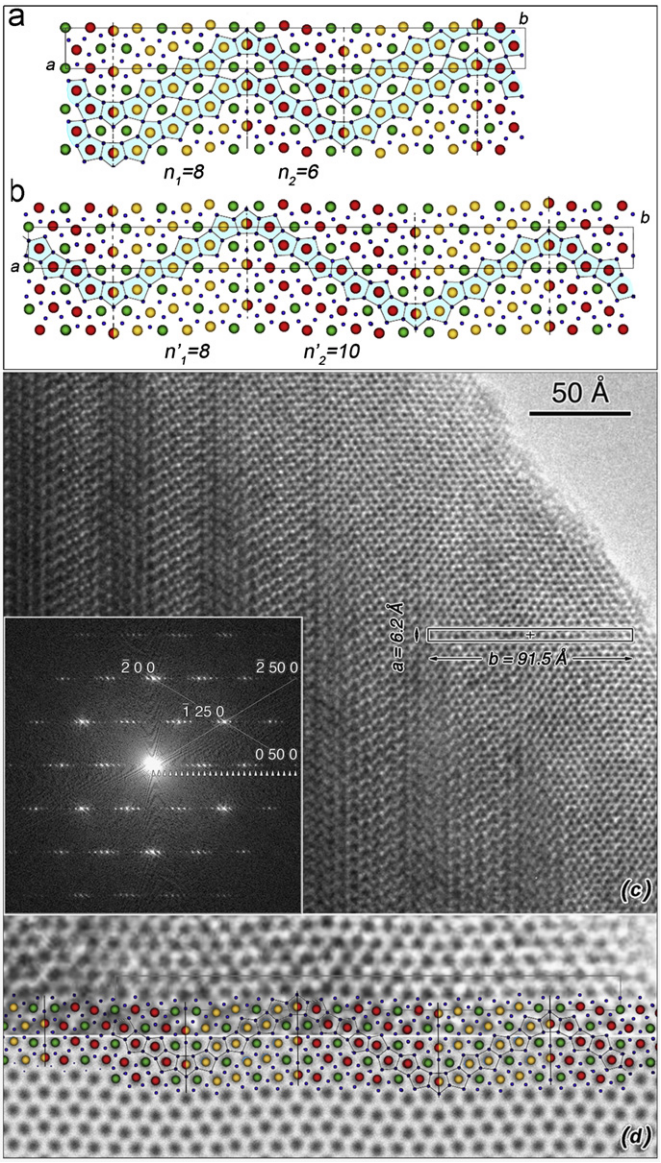

Fig. 2. Atomic structures of: (a) 19L-Ta_2O_5 in projection along [001]; (b) structural model for 25L-Ta_2O_5 deduced from crystallographic data and structural rules of Grey et al. [6] (see text for the structural description); (c) HRTEM image of [001] zone axis with its FFT in inset, showing a strong change in the contrast of fringes with the sample thickness; and (d) comparison between an enlarged image of (c) on the thin sample edge and a simulated image. The projection of the 25L-Ta_2O_5 structural model along [001] indicates that dots of dark contrast correspond to columns of Ta–O atoms. (For interpretation of the references to color in this figure legend, the reader is referred to the web version of this article.)

C-centering (Fig. 2(b)).[2] Note that if both cell parameters b of 19L- and 25L-Ta_2O_5 correspond to $19b_0$ and $25b_0$, respectively, the distance $b_0/2$ corresponds only to an average distance between the successive planes of Ta atoms parallel to (010). Along the [010] direction, Ta atoms form two types of zig-zag rows which are best seen at a glancing angle.

A HRTEM image of a fragment oriented along a [001] zone axis is shown in Fig. 2(c). The structure of 25L-Ta_2O_5 and its [001] orientation was verified from the FFT of the image shown in inset. The focalization of the objective lens was close to the condition of Scherzer defocus $\Delta f = -1.2(C_s\lambda)^{1/2} = -42.5$ nm for a spherical aberration coefficient $C_s = 0.5\ 10^6$ nm and an electron wavelength $\lambda = 2511 \times 10^{-6}$ nm. One observes that the contrast of fringes is changing very rapidly with an increase in the sample thickness. In particular, the contrast variation is increasingly pronounced at periodicity of $b/2$ in the thicker sample part. An enlarged image of the sample edge is compared to a simulated image and to the positions of the [001] atomic columns in Fig. 2(d). Image simulations were performed by the multi-slice method using the "JEMS" program [17]. Atomic columns Ta–O correspond to black dots while O columns are not visible. At a glancing angle along the [010] axis, the zig-zag rows of Ta–O columns appear to be similar between both simulated and HRTEM images. Similar types of simulated images were, however, only obtained for a thickness up to 1.2 nm and defocus values in a range of −21.5 to −25 nm, which were not close to the Scherzer defocus of −42.5 nm. Moreover, by increasing the crystal thickness, it was not possible to obtain simulations in agreement with the observed contrast of fringes, in particular, a reinforcement of contrast at a period of $b/2$.

The Fig. 3(a) and (b) shows $\theta/2\theta$ X-ray powder diffraction patterns of the initial Ta_2O_5 product and the rapidly cooled

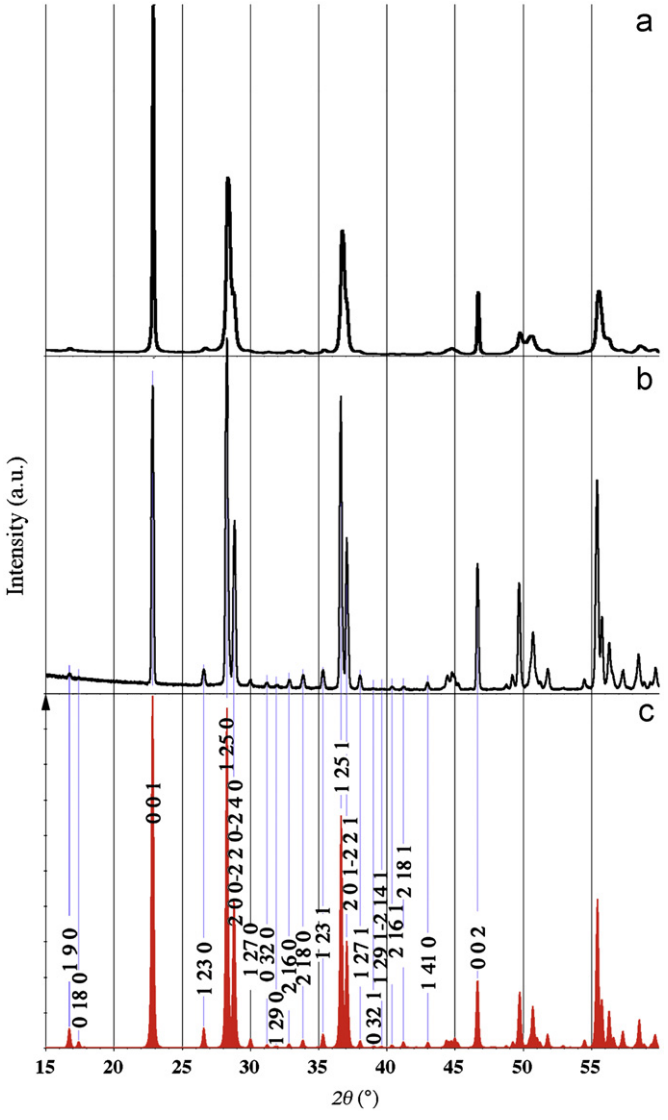

Fig. 3. Comparison between $\theta/2\theta$ X-ray powder diffraction diagrams of: (a) the initial Ta_2O_5 product, (b) the rapidly cooled sample after a sintering at 1210 °C and annealing at 1000 °C for 1 h and (c) a simulation of the X-ray diagram of the model of 25L-Ta_2O_5 structure shown in Fig. 2(b). (For interpretation of the references to color in this figure legend, the reader is referred to the web version of this article.)

[2] As the cell contains 50 Ta and 132 O sites, Ta interstitials ($Ta_{52.8}O_{132}$) or oxygen vacancies ($Ta_{50}O_{125}$) have to be considered in order to fit a Ta_2O_5 stoichiometry.

sample after a sintering at 1210 °C and annealing at 1000 °C for 1 h, respectively. Both these diagrams are compared to a simulation of the X-ray diagram of the model of 25L-Ta_2O_5 structure (Fig. 3(c)). The simulation was performed using the computer program "Carine" [18] where a Debye–Waller temperature factor of 2 Å^2 has been fixed for all the atoms. The diagram of the initial product shows just a few similarities with the simulation while a reasonable agreement can be observed between the diagram of the rapidly cooled sample and the simulation. The peak positions correspond to those calculated and their relative intensities are quite similar. There is, however, an important background which will be shown to be related to diffuse scattering (Section 3.2). Let us note that the initial Ta_2O_5 powder was found to be inhomogeneous from a few TEM investigations. SAED patterns of [001] zone axes that we have observed were characteristic of grains of different structures: 11L-Ta_2O_5, 14L-Ta_2O_5 and an incommensurate phase derived from 25L-Ta_2O_5. But, as after sintering at 1210 °C, a homogeneous state of 25L-Ta_2O_5 structure was observed by TEM to be similar to the state observed after annealing at 1000 °C for 1 h, followed by rapid cooling, we can conclude that the mixed structure of the initial powder was transformed between 1000 and 1210 °C.

3.2. Satellite reflections related to a commensurate superstructure

Discrepancy between simulated and observed HRTEM images of [001] zone axis must be sought in the understanding of the diffuse scattering localized in planes normal to the [001] axis at about $\pm\mathbf{c}^*/6$ from the 0 0 l reflections. The Fig. 4(a) shows a set of four electron diffraction patterns observed in a rapidly cooled sample, where the three patterns of [100], [910] and [010] zone axes and exhibiting diffuse scattering, are related by rotations of 90° to the pattern of [001] zone axis. From these patterns, one determines that the diffuse scattering is localized on parallel lines of [010] direction and passing through points of coordinates $x^*=\frac{1}{2}ha^*$, $y^*=0$, $z^*\simeq(l\pm\frac{1}{6})c^*$. Two types of line are distinguished from both first order Laue zone at about $\pm\mathbf{c}^*/6$ (Fig. 4(b)):

- for $x^*=na^*$ ($n\in\mathbb{Z}$) the maxima of diffuse scattering intensity along [010] are centered on lattice points of coordinates $x^*=ha^*$, $y^*=9(1+2k)b^*$, $z^*\approx(l\pm\frac{1}{6})c^*$ from each reflection of the Lehovec sub-cell (i.e. 0 5 0 0, 2 5 0 0, 1 2 5 0, 2 0 0, 0 0 1, …). This gives rise to multiple scattering effects, as the one indicated on the pattern of [100] zone axis between the transmitted beam and the reflection 0 5 0 0.
- for $x^*=\frac{1}{2}na^*$ (n odd), the maxima of diffuse scattering intensity along [010] are localized on a sub-lattice quite similar to this of fundamental reflections. This lattice is translated in opposite directions by vectors $\pm(\frac{1}{2}a^*,0,\approx\frac{1}{6}c^*)$, i.e. an inversion through the origin of the reciprocal lattice, which implies a lattice of satellite reflections of lower symmetry than the reciprocal lattice of the Lehovec sub-cell.

The positions of these intensity maxima correspond to reflections of a superstructure of the Lehovec sub-cell. The associated reciprocal lattice is spanned by vectors $\mathbf{b}_s^*=\frac{9}{25}\mathbf{b}_0^*$ and $\mathbf{c}_s^*\approx\frac{1}{6}\mathbf{c}_0^*$. The $\mathbf{a}_s^*$ vector remains undetermined but its projection onto the [100] axis is equal to $\frac{1}{2}\mathbf{a}_0^*$. In this case, the ($hkl$) fundamental reflections of the 25L-Ta_2O_5 structure have an index $k=2p=50q+18r$ for h, $k=2n$ ($p,q,r,n\in\mathbb{Z}$) since they are generated by multiple scattering effects between reflections of the Lehovec sub-cell and the superstructure along the [010] direction. These reflections are periodic along the [010] direction if b_0/b_s is exactly equal to the rational fraction $\frac{9}{25}$, i.e. $2\mathbf{b}^*=3\mathbf{b}_s^*-\mathbf{b}_0^*=\frac{2}{25}\mathbf{b}_0^*$ where

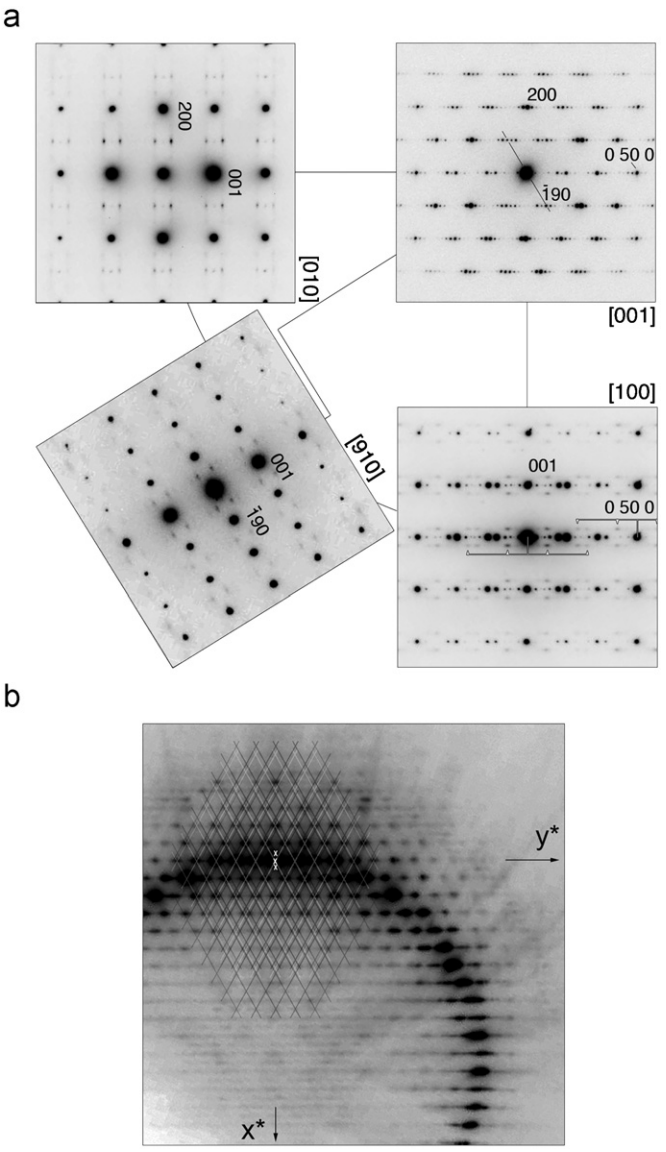

Fig. 4. (a) Set of SAED patterns of [100], [010], [001] and [910] zone axes observed in a rapidly cooled sample and exhibiting a diffuse scattering located in planes normal to the z^* axis and at about $\pm\mathbf{c}^*/6$ from 0 0 l reflections; (b) ($00\approx\pm c^*/6$) first order Laue zone observed on a SAED pattern of zone axis close to [001]. There are two types of diffuse scattering lines parallel to y^* axis at na^* and $\frac{1}{2}na^*$ $n\in\mathbb{Z}$. Both ($00\approx+c^*/6$) and ($00\approx-c^*/6$) first order Laue zones appear to be related by a symmetry of inversion from the grid of white lines superimposed to the intensity maxima of the fundamental reflections and the two grids of black lines superimposed to intensity maxima of the diffuse scattering lines at $\frac{1}{2}na^*$.

$b=\frac{1}{b^*}$ is the cell parameter of 25L-Ta_2O_5. Obviously the structure will be incommensurate along the [010] direction for an irrational fraction b_0/b_s. But, how to qualify the structure when the fraction b_0/b_s is apparently equal to $\frac{9}{25}$? In this case, the structure can be considered as commensurately modulated as long as satellite reflections characteristic of a superstructure can determined within the diffuse scattering (i.e. what would be actually the case here). If not, it is the periodic 25L-Ta_2O_5 structure. A diffuse scattering can nevertheless remain due, for instance, to Ta interstitials or oxygen vacancies. Thus, if the satellite reflections are changing as a function of temperature, a continuous or second order incommensurate phase transition can be assumed to occur. In order to examine a possibility of a phase transition, other annealing treatments could be performed because samples observed by TEM were found to be single phase; The property

of single phase allows one to consider that a phase transition would be of second order. Results on this study are reported in the next Section 3.3.

Several features observed on HRTEM images can be associated with the diffuse scattering (Fig. 5). The HRTEM image (a), shown at low magnification, was taken on a fragment rapidly cooled down. The zone axis of observation is [100] from an indexing of the corresponding FFT of this image (Fig. 5(b)). As it exhibits features corresponding to the diffuse scattering previously observed on the SAED pattern of [100] zone axis (Fig. 4(a)), the image (a) contains information at the origin from the diffuse scattering. There are contrast variations resulting of structural modulations: large fluctuations along [001] and a periodic variation of contrast along [010] corresponding to the b cell parameter of the 25L-Ta_2O_5 structure. At higher magnification (Fig. 5(c)) variations in the fringe contrast appear to be in agreement with the superstructure previously deduced from electron diffraction patterns. Domains in dark gray contrast correspond to the ordered superstructure of periodic parameters $\approx\frac{1}{9}b$ and $\approx 6c$ (see inset) while domains of clear gray contrast seem to be less ordered. Such a modulated state along the c-axis implies that Ta–O atomic columns must be distorted. Therefore, it justifies the fact that beyond a certain critical thickness, HRTEM images of crystal fragments oriented along a [001] zone axis cannot be simulated from the structural model 25L-Ta_2O_5.

We have verified several times that HRTEM observations of very thin samples oriented along a [001] zone axis showed a good agreement with the x, y coordinates of the Ta atoms of the 25L-Ta_2O_5 model. Although it cannot be excluded that a structural relaxation might occurs in very thin crystals, it seems that x, y coordinates of Ta atoms in the superstructure almost correspond to those of the 25L-Ta_2O_5 model. In this case, the structural differences could mainly be on the atomic positions of oxygen, although shifts of Ta atoms along z can also be considered. Shifts along z imply, however, a non-centrosymmetric space group $C112$ or $C11m$ with respect to $C112/m$. Let us recall that in Ta_2O_5 thin films deposited on different substrates, several authors have identified a property of piezoelectricity [20–24]. For instance, Parmentier et al. [24] have found by X-ray diffraction and interferometric measurement of piezoelectric displacement that a textured layer of 11L-Ta_2O_5 structure (also called β–Ta_2O_5) is piezoelectric, which is a proof of a non-centrosymmetric space group (e.g. $P112$ with a polar axis [001] if the reflection conditions correspond to those of the centrosymmetric space group $P112/m$). A similar result was obtained by Looste and Viljoen [23].

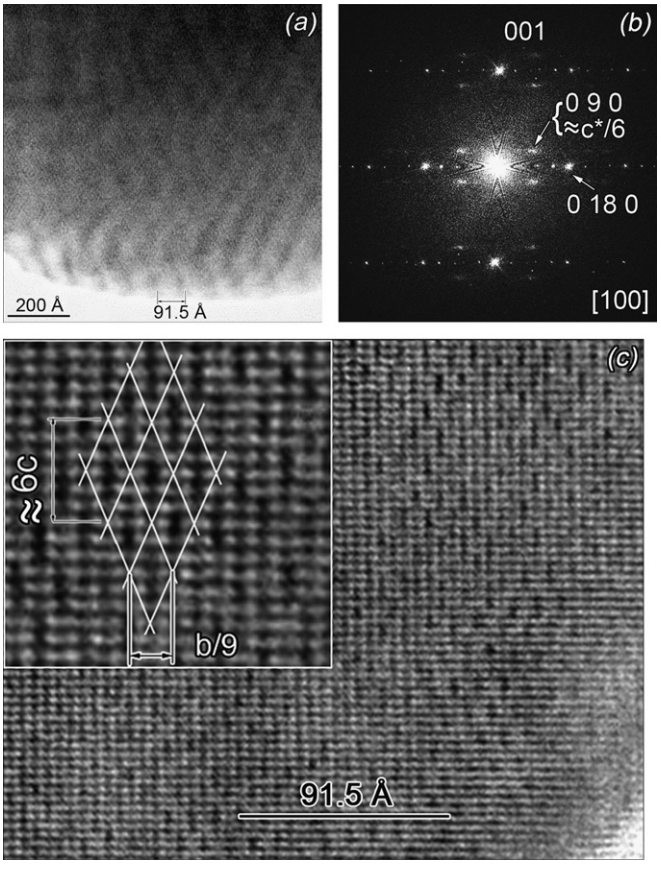

Fig. 5. (a, b) HRTEM image and corresponding FFT of the image showing the structural modulation of 25L-Ta_2O_5 rapidly cooled down from 1000 °C and which from the enlarged image (c) appear to be the result of a partial formation of an incommensurate superstructure of parameters $\approx\frac{1}{9}b$ and $\approx 6c$ along the [100] zone axis.

3.3. Phase transition

The 25L modulated structure evolves as a function of the cooling rate. The three diffraction patterns of [100] zone axis shown in Fig. 6(a) correspond from left to right to samples cooled down from 1000 °C at rates of 5, 1 and 0.1 °C min^{-1}. The satellite reflections become more intense and their number increases as the cooling rate decreases. The splitting of reflections marked by arrows on the SAED pattern on the right correspond to satellites from both transmitted and 0 0 1 diffracted beams. It indicates that the period c_s of the superstructure is incommensurate with the c period of 25L-Ta_2O_5. From measurements on this pattern the c_s cell parameter of the superstructure is about equal to $6.33c$. Both Fig. 6(b) and (c) are related to the sample cooled down at 0.1 °C min^{-1}. They show, respectively, in (a) a set of four electron diffraction patterns (like in Fig. 4, for comparison) and in (b) the first order Laue zone at $+\mathbf{c}_s^*$ along the [001] zone axis. From these figures, one deduces that dense sets of satellite reflections are along lines parallel to [010] and passing through points of coordinates $x^*=\frac{1}{2}ha^*$, $y^*=0$, $z^*\approx(l\pm n/6.33)c^*$ (with $n=1, 2$). The rows of reflections parallel to [010] are no longer periodic. Such a departure from periodicity is observed in Fig. 6(d) corresponding to an enlarged part of the $1\,k\,0$ row of reflections observed along the [001] zone axis in Fig. 6(b). Therefore, an incommensurate modulation occurs along the [010] axis. According to the previous analysis (Section 3.2), the reflections of both subsystems of the incommensurate basic structure can be derived from reflections of the Lehovec cell[3] (e.g. $1\,1\,0_0$ previously indexed as $1\,25\,0$ for 25L-Ta_2O_5) and the reflections of the superstructure, (e.g. $0\,2\,0_s$ corresponding to vector $2\mathbf{b}_s^*$ and previously indexed as 190 in the case of 25L-Ta_2O_5) (Fig. 6(d)). The row of reflections are not periodic along the [010] direction because b_0/b_s is irrational. From the Fig. 6(d) one can deduces that $|d^*|=|3b_s^*-b_0^*|$ and $|\delta^*|=|8b_0^*-22b_s^*|$. From measurements and assuming that $b_0=3.66$ Å, one finds $d_{0\,1\,0s}=10.22$ Å, instead of 10.17 Å for the superstructure observed after a rapid cooling.

Note that the reflections of superstructure observed along the [001] axis on the SAED pattern of [100] zone axis in Fig. 6(b) are the result of double diffraction because they are not observed on the other patterns of [010] and $[1\nu\ 0]$ zone axes. Both these last patterns exhibit satellite reflections and important diffuse scattering which, from a rotation of about 30° around the [001] axis, was observed to be limited by planes at $(00l\pm c_0^*/6.33)$. In direct space, such diffuse scattering must be characteristic of a

[3] "Cell" is used instead of "sub-cell" because the Lehovec cell cannot be a sub-cell for the incommensurate phase.

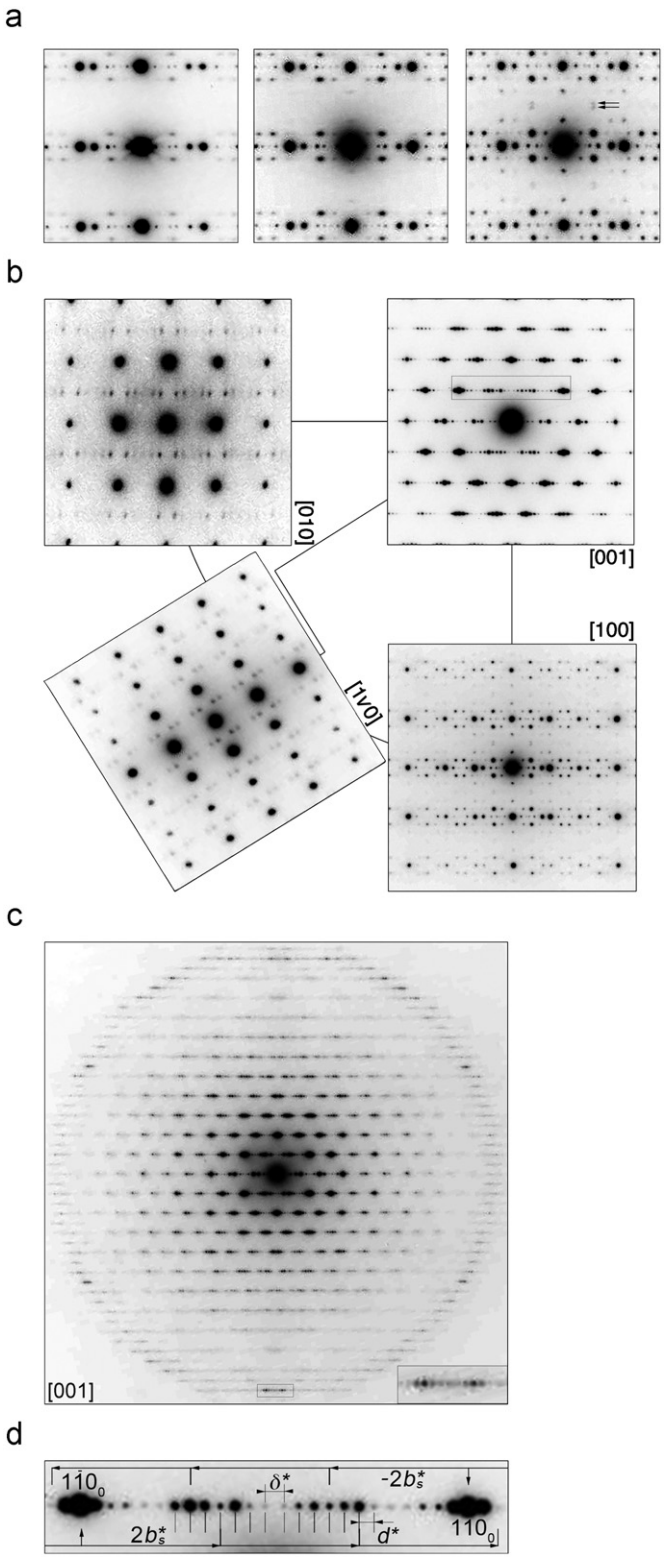

Fig. 6. (a) SAED patterns of [100] zone axis corresponding from left to right to Ta_2O_5 samples cooled down from 1000 °C at rates of 5, 1 and 0.1 °C min^{-1}, (b) set 4 SAED patterns of the sample cooled like in Fig. 4, (c) first order Laue zone at *about* $+\mathbf{c}^*/6$ and (d) enlarged part of the array of 1 *k* 0 reflections observed along the [001] zone axis in (b) (see text).

translational disorder along the [001] axis. As these planes are repeated on either sides of 0 0 *l* reflections of the Lehovec cell, the c_s/c_0 ratio must tend to a limit corresponding to a rational fraction $c_s/c_0 \leq \frac{19}{3}$.

The third parameter a_s of the incommensurate superstructure can be determined from a reciprocal plane containing a periodic array of both types of satellite rows parallel to [010]. The Fig. 7(a) shows a SAED pattern of zone axis very close to $[201]_0$ of the Lehovec cell ($020_0, 1\bar{1}\,\bar{2}_0, 11\bar{2}_0, 20\bar{4}_0$) and rows of satellite reflections parallel to [010]. These rows are indexed as a function of their x^*, z^* coordinates in Fig. 7(a). Three of these rows, namely (a_0^*, $2c_0^*-c_s^*$), ($3a_0^*/2, 3c_0^*-c_s^*$) and ($2a_0^*$ $4c_0^*-c_s^*$) are quite close to Bragg's condition of diffraction. The row at ($3a_0^*/2, 3c_0^*-c_s^*$) exhibits discrete reflections when it is placed in an exact condition of diffraction (inset in the bottom part of Fig. 7 (a)). For the type of row at $x^* = \frac{1}{2}na_0^*$ (n odd) there is an inversion through the origin between the rows at $+c_s^*$ and $-c_s^*$, as previously observed on the sample rapidly cooled (Fig. 4(b)). These rows exhibit an overall periodicity of reflections of b_s^* along the [010] axis (see inset). A periodic 2D lattice of satellites, spanned by vectors $2\mathbf{b}_s^*$ and $2\mathbf{q}^*$ almost parallel to the plane of the figure, can be defined from reflections along both types of rows at $+c_s^*$. This lattice is characteristic of a 2D centered oblique cell. There is a symmetrical lattice to this one through a (010) mirror plane, which implies that the number of reflections along the rows at $x^* = \frac{1}{2}na_0^*$ is twice the number of reflections along rows at $x^* = na_0^*$.

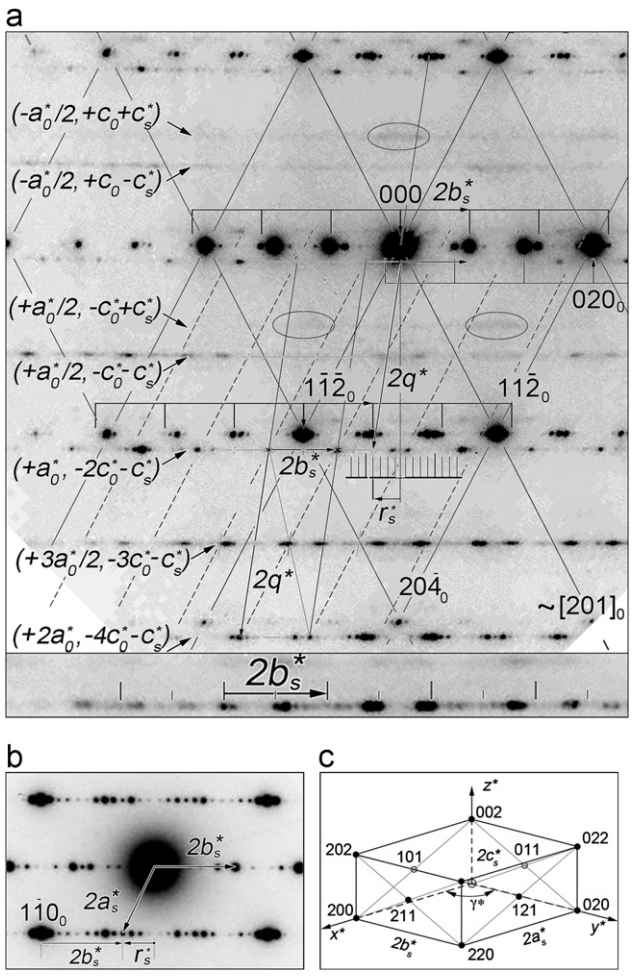

Fig. 7. (a) and (b) SAED patterns of [201] and [001] zone axes from whose the vector $2\mathbf{a}_s^*$, the reciprocal unit cell of the superstructure, shown in (c), and its space group can be determined (see text).

The coordinates of the $2\mathbf{q}_s^*$ vector corresponds to $\frac{1}{2}(2,0,\overline{4})_0$ and $\mathbf{r}_s^*$. The projection of $\frac{1}{2}(2,0,\overline{4})_0$ on the x^* axis is equal to $\mathbf{a}_0^*$. From the previous analysis shown in Fig. 6(d), the vector $\mathbf{r}_s^*$ has a length of $|r_s^*| = 3|d^*| + \frac{1}{2}|\delta^*| = |b_0^* - 2b_s^*|$. If $2\mathbf{a}_s^*$ corresponds to the projection of $2\mathbf{q}_s^*$ onto the reciprocal plane x^*,y^*, then the 3D reciprocal lattice of the superstructure corresponds to this of a monoclinic system (Fig. 7(c)). In this case, the condition of reflections correspond to those of the space group $I2/a$ (z-axis unique) [19], i.e. $h\,k\,l$: $h+k+l=2n$, $h\,k\,0$: h, $k=2n$.

The cell parameters are:

- $\gamma_s = 64.53^\circ$, with $\gamma_s^* = \pi - \gamma_s = (\pi/2) + \arctan(b_0^* - 2b_s^*)/a_0^* = 115.67^\circ$.
- $a_s = 12.4\,\text{Å} = (1/a_s^*)\sin\gamma$, with $a_s^* = \frac{1}{2}((a_0^*)^2 + (b_0^* - 2b_s^*)^2)^{1/2}$.
- $b_s = 11.32\,\text{Å} = 1/b_s^* \sin\gamma$, with $1/b_s^* = d_{0\,1\,0s} = 10.22\,\text{Å}$.
- $c_s = 24.64\,\text{Å} = 6.33c_0$

Note, however, that such a monoclinic structure implies a discrepancy with the previous remark that the reflection $0\,0\,2_s$ results of a double diffraction effect. This is due to the fact that the superstructure is not exactly monoclinic but triclinic, as shown after from a HRTEM observation (Fig. 9).

A comparison of the $\theta/2\theta$ X-ray powder diffraction diagram of the sample cooled down at $0.1\,^\circ\text{C}\,\text{min}^{-1}$ from $1000\,^\circ\text{C}$ with the simulation of X-ray powder diagram of the 25L-Ta_2O_5 structural model is shown in Fig. 8. The reflections of strong intensity, which correspond to those of the Lehovec cell (see indexing) remain at the same 2θ values than those of 25L-Ta_2O_5, while very small shifts can be observed for reflections of small intensity. The background intensity has to be related to the diffuse scattering previously observed by TEM. Any additional reflection with respect to those of the 25L-Ta_2O_5 structure are not distinguished, such as those observed by SAED. Note that if the vector $(1,1,0)_0$ remains invariant through the phase transition, one deduces from $2\mathbf{a}_s^* = \mathbf{a}_0^* + \mathbf{b}_0^* - 2\mathbf{b}_s^*$ that $\mathbf{a}_s^*$ varies with $\mathbf{b}_s^*$.

The Fig. 9(a) shows a HRTEM image of $[100]_0$ zone axis of the sample slowly cooled at $0.1\,^\circ\text{C}\,\text{min}^{-1}$. The FFT of the image (in inset) is similar to SAED patterns previously shown in Fig. 6(a) and (b). The contrast variations are therefore characteristic of the incommensurate basic structure composed of the mutually incommensurate Lehovec and superstructure subsystems. The

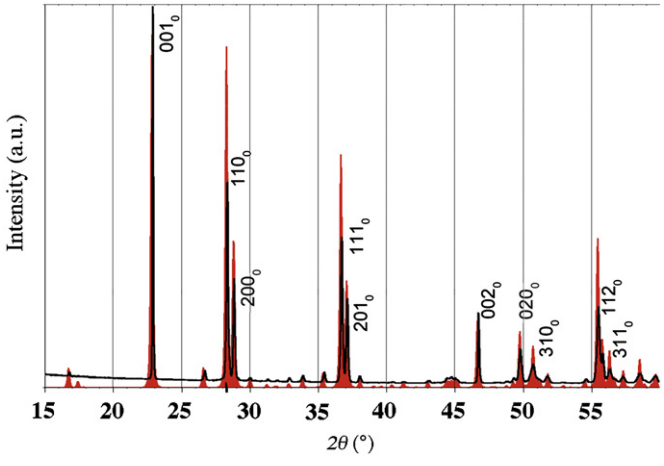

Fig. 8. Comparison between the $\theta/2\theta$ X-ray powder diffraction diagram of the sample cooled down at $0.1\,^\circ\text{C}\,\text{min}^{-1}$ from $1000\,^\circ\text{C}$ and the simulation of the X-ray diagram of the 25L-Ta_2O_5 model (in red). The C-centered orthorhombic sub-cell of Lehovec is indexed. (For interpretation of the references to color in this figure legend, the reader is referred to the web version of this article.)

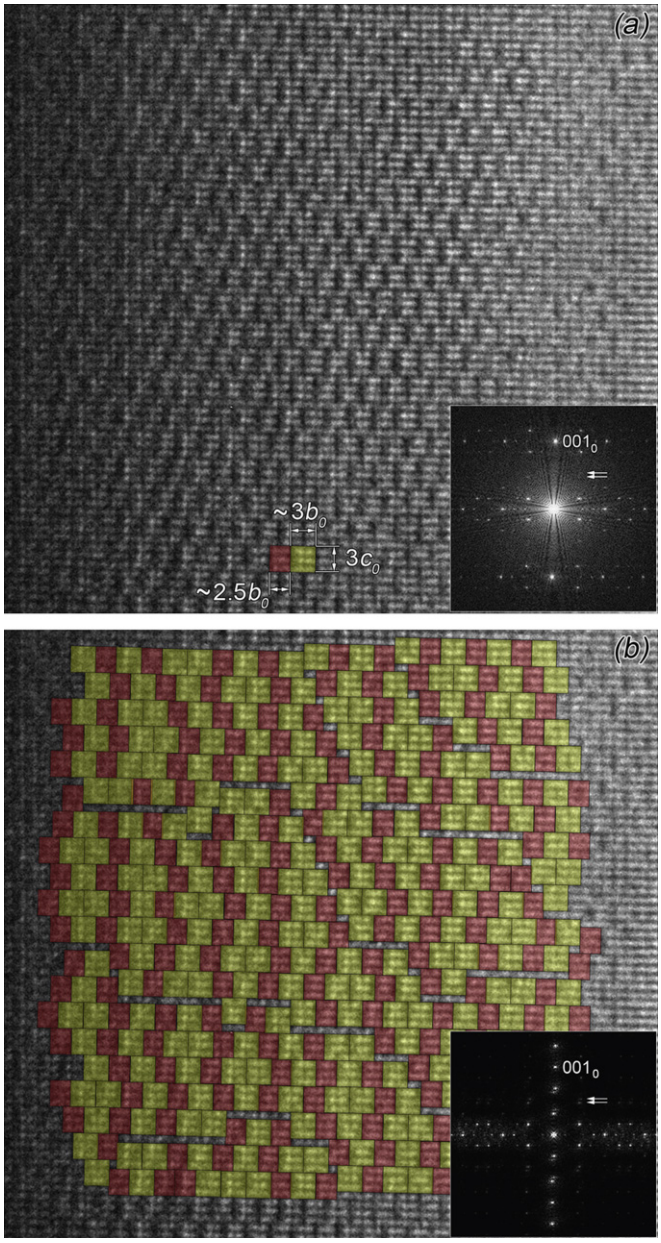

Fig. 9. (a) HRTEM image of $[100]_0$ zone axis and its FFT of the sample slowly cooled at a rate of $0.1\,^\circ\text{C}\,\text{min}^{-1}$. Two types of tile in red and yellow color are defined from the fringe contrast; (b) tiling superimposed to the image (a) and FFT corresponding to the tiling only. (For interpretation of the references to color in this figure legend, the reader is referred to the web version of this article.)

vertical segments in dark contrast are nearly $3c_0$ length. They are similar to those observed in Fig. 5(c). Along the horizontal direction ($[010]_0$) they are spaced by distances of either $\approx 2.5b_0$ or $\approx 3b_0$. On account of a c_0 value of 3.89 Å, the measured distances are 9.25 ± 0.05 Å and 11.1 ± 0.05 Å, i.e. very close to $2.5b_0 = 9.15$ Å and $3b_0 = 10.98$ Å. Two types of rectangular tiles are defined in red and yellow colors in order to superimpose a tiling to the image (Fig. 9(b)). As a result, it appears that large modulations occur along the $[001]_0$ axis. The period of modulation is variable: the main period is $6c_0$ and sometimes $12c_0$. There are also stacking defects of thickness c_0, more or less extended in the direction $[010]_0$. Along vertical lines these defects occur in an average ratio of distance close to $\frac{1}{18}$. They create therefore a disorder along $[001]_0$ which can be related to the

diffuse scattering limited by planes at $(00l \pm c_0^*/6.33)$ (Fig. 6(b)). These defects seem to be due to an incommensurate superstructure not exactly monoclinic but triclinic. Actually the $0\,0\,1_0$ fringes are not perpendicular to the vertical direction of the modulation. There is a departure of about 1.4° with respect to $\pi/2$. From observations on two other fragments we have also found angular departures of about 1.4° and 1.5° as well as stacking defects in average ratios of distance close to $\frac{1}{18}$. The FFT of the tiling alone (inset of Fig. 9(b)) exhibits a frequency spectrum similar to this of the FFT of the HRTEM image in (a): one finds frequencies of the Lehovec cell superimposed to frequencies of the incommensurate superstructure with, in particular, a splitting of spots (pointed by arrows) characteristic of the ratio $c_0^*/c_s^* = 6.33$. The period $d_{0\,1\,0s} = b_s \sin\gamma$ along the $[010]_0$ direction is in between $2.5b_0$ and $3b_0$ and represents an average period related to p yellow tiles and q red tiles such that:

$$b_s \sin\gamma = \frac{(3p+2.5q)b_0}{p+q}$$

with p, q integers.

On account of the b_0, b_s and γ values, one obtains $p/q = 1.4073 \approx \frac{7}{5}$. For an exact ratio of $\frac{7}{5}$, $b_s \sin\gamma$ would be equal to 10.2175 Å instead of 10.22 Å. A difference which is below the measurement accuracy (i.e. about ± 0.05 Å).

Let us remark that both widths of tile, $2.5b_0$ and $3b_0$, can be related to the m values of all commensurate m L-Ta_2O_5 structures since m can be expressed as $(3p+2.5q)b_0$ for $m = 5, 8, 11, 13, 14, 19, 25$. Conversely, a ratio $p/q = \frac{7}{5}$ can be related to a m value of 67 corresponding to a sequence of folded chain of edge shared TaO_7 bipyramids of 22-24-22-24. Such widths seem therefore to indicate a possibility of similar local transformations in all the atomic structure of L-Ta_2O_5 phases. From HRTEM observations of $[001]_0$ zone axis on very thin fragments slowly cooled at 0.1 °C min^{-1} we have observed patterns of black dots very similar to the one shown in Fig. 2(b) and (c). This indicates that the x, y coordinates of Ta atoms remain similar to those of the 25L-Ta_2O_5 model after transformation into an incommensurate structure.

4. Discussion and conclusion

In summary, the present results shows that a single phase of 25L-Ta_2O_5 commensurate modulated structure, obtained at high temperature, transforms into an incommensurate modulated structure through very slow cooling. A second order incommensurate phase transition can be assumed to occur in this case. When rapidly cooled, the 25L-Ta_2O_5 atomic structure does not fit perfectly to a periodic model determined from structural rules and crystallographic data on 19L-Ta_2O_5 published by Grey et al. [6]. The phase exhibits weak diffuse scattering corresponding mainly to modulations with components in the three directions of space. Actually, such modulations are due to a formation of a superstructure of the Lehovec sub-cell [8]. The relations between the cell parameters of the superstructure and the Lehovec sub-cell are: $a_s \sin\gamma = 2a_0$, $b_s = \frac{25}{9}b_0$, and $c_s \approx 6c_0$. A modulation along the c-axis allows one to understand why HRTEM images of [001] zone axis cannot be simulated beyond a sample thickness of about 1.2 nm. Through a very slow cooling, the superstructure becomes more developed and its cell parameters are slightly changing while the Lehovec cell remains apparently invariant. From SAED results, the incommensurate superstructure is determined to be monoclinic of space group $Ia/2$. But as the actual superstructure appears to be triclinic from HRTEM images, stacking defects along the c-axis are formed through the continuous phase transition. In this case, the cell parameter c_s becomes equals to about $6.33c_0$. An interpretation of this c_s value, obtained from a tiling superimposed to the contrast of fringes of a HRTEM image of [100] zone axis, is that stacking defects of c_0 thickness occurs on an average distance of $18 \times c_0$. The ratio b_s/b_0 is no longer equal to a rational fraction $\frac{25}{9}$ characteristic of the 25L structure, which implies that the transition is incommensurate along the [010] axis. Along the b-axis, the tiling with two rectangular tiles of dimensions $3b_0 \times 3c_0$ and $2.5b_0 \times 3c_0$ seems to occur on long distances without defect. Such $3b_0$ and $2.5b_0$ subunits could be related to all m L-Ta_2O_5 structures since all the m values found so far can be expressed as $m = 3p+2.5q$, with p,q integers.

From several works of Schmid and colleagues [9,10,16,25], we think that similar phase transitions could likely occur in the system $(1-x)$ Ta_2O_5, x WO_3. These authors have studied by X-ray single-crystal diffraction, several commensurate and incommensurate structures in a range of composition $0 \le x \le 0.267$. An advantage of this system is that single crystal samples, suitable for X-ray diffraction on 4-circles goniometer, can be obtained. However, as the cooling conditions of their samples are not mentioned [10,16], one can assume that they were more or less rapid (i.e. compared to a cooling rate of 0.1 °C min^{-1}). Among different approaches developed by Schmid et al., one of them [9] is based on incommensurately modulated structures in a (3+1)-dimensional superspace [26–28]. Refinements of X-ray single-crystal diffraction data have been performed on three samples of compositions $x = 0.1$, 0.14 and 0.267. Two components substructures have been considered:

(i) a metal-substructure constituted of metal atoms and oxygen atoms located at the apices of the metal-atom coordination polyhedra (i.e. at $z = \pm\frac{1}{2}$); the cell parameters of this metal-substructure correspond to those of the Lehovec cell ($a_M = a_0$, $b_M = b_0$, $c_M = c_0$) and
(ii) an oxygen-substructure formed by oxygens at $z = 0$ ($a_{Ox} = a_M$, $b_{Ox} = b_M/1.628$, $c_{Ox} = c_M$).

A superspace group of symmetry has been determined from diffraction data in order to perform refinements of the atomic modulation functions. Thus, unlike current results, both a and c axes have been considered as invariant. Only the b sub-lattice parameters are mutually incommensurable. Although Schmid et al. [9] have obtained satisfactory values in weighted reliability factors, they noted discrepancies on two points:

(i) "An apparent contradiction between the bond-valence requirements of the metal atoms and the thermal parameter modulation trend". (The bond-valence requirements are that either Ta interstitials [6,29] or oxygen vacancies [16,9] must be considered with respect to stoichiometries implied by full occupancy of all the refined atomic positions.)
(ii) "Unsatisfactory fit to the first-order satellite reflections compared with the main, second- and third-order satellite reflections" for all the sample compositions.

About this second point, Schmid et al. [9] mention that TEM studies [10,16] have revealed the presence of considerable diffuse intensity which becomes more structured and more pronounced on going from $x = 0.267$ to 0.1. It is noted that the sharpening in the diffuse pattern apparently correlates to a worsening fit of the first-order satellites. This diffuse scattering is comparable to the one presently observed. However, it is located in planes normal to [001] at either $c^*/12$ or $c^*/8$ as a function of their structure ($m = 8$ and 13, resp.) and/or composition ($x = 0.267$ and 0.14 resp.) [16]. On account of these TEM results, it seems to us that incommensurate phase transitions could likely occur in the system Ta_2O_5–WO_3.

References

[1] R.S. Roth, N.C. Stephenson, in: L. Eyring, M. O'Keeffe (Eds.), The Chemistry of Extended Defects in Non-Metallic Solids, North-Holland, Amsterdam1970, pp. 167–181.
[2] N.C. Stephenson, R.S. Roth, Acta Crystallogr. B 27 (1971) 1010–1017.
[3] N.C. Stephenson, R.S. Roth, Acta Crystallogr. B 27 (1971) 1018–1024.
[4] N.C. Stephenson, R.S. Roth, Acta Crystallogr. B 27 (1971) 1031–1036.
[5] N.C. Stephenson, R.S. Roth, Acta Crystallogr. B 27 (1971) 1037–1044.
[6] I.E. Grey, W.G. Mumme, R.S. Roth, J. Solid State Chem. 178 (2005) 3308–3314.
[7] S. Lagergren, A. Magneli, Acta Chem. Scand. 6 (1952) 444–446.
[8] K. Lehovec, J. Less-Common Metals 7 (1964) 397–410.
[9] S. Schmid, K. Fütterer, J.G. Thompson, Acta Crystallogr. B 52 (1996) 223–231.
[10] S. Schmid, R.L. Withers, J.G. Thompson, J. Solid State Chem. 99 (1992) 226–242.
[11] T. Miyano, J. Solid State Chem. 126 (1996) 208–220.
[12] Q. Fang, J.-Y. Zhang, Z.M. Wang, J.X. Wu, B.J. O'Sullivan, P.K. Hurley, T.L. Leedham, H. Davies, M. Audier, C. Jimenez, J.-P. Senateur, I.W. Boyd, Thin Solid Films 428 (2003) 248–252.
[13] A. Lintanf-Salaun, A. Mantoux, E. Blanquet, E. Djurado, J. Electrochem. Soc. 156 (2009) H311–H315.
[14] A. Lintanf-Salaun, Thesis, Dépots par ESD et ALD et caractérisations physico-chimiques de couches d'oxydes á l'échelle nanométrique pour la microélectronique, INP-Grenoble, 2008.
[15] C. Askeljung, B. Marinder, M. Sundberg, J. Solid State Chem. 176 (2003) 250–258.
[16] S. Schmid, J.G. Thompson, A.D. Rae, B.D. Butler, R.L. Withers, N. Ishizawa, S. Kishimoto, Acta Crystallogr. B 51 (1995) 698–708.
[17] P. Stadelmann, Java electron microscope simulation software 〈http://cimewww.epfl.ch/people/stadelmann/jemsWebSite/jems.html〉.
[18] C. Boudias, D. Monceau, Carine crystallography 3.1, software for research and teaching, Copyright 1989–2005.
[19] Hypertext Book of Crystallographic Space Group, Copyright 1997–1999, Birkbeck College, University of London 〈http://img.chem.ucl.ac.uk/sgp/mainmenu.htm〉.
[20] Y. Nakagawa, Y. Gomi, Appl. Phys. Lett. 46 (1985) 139–140.
[21] Y. Nakagawa, Y. Gomi, T. Okada, J. Appl. Phys. 61 (1987) 5012–5017.
[22] Y. Nakagawa, T. Okada, J. Appl. Phys. 68 (1990) 556–559.
[23] B.R. Jooste, H.J. Viljoen, J. Mater. Res. 13 (1998) 475–482.
[24] R. Parmentier, F. Lemarchand, M. Cathelinaud, M. Lequime, C. Amra, S. Labat, S. Bozzo, F. Bocquet, A. Charai, O. Thomas, C. Dominici, Appl. opt. 41 (2002) 3270–3279.
[25] A.D. Rae, S. Schmid, J.G. Thompson, R.L. Withers, N. Ishizawa, Acta Crystallogr. B 51 (1995) 709–721.
[26] A. Janner, T. Janssen, Phys. Rev. B 15 (1977) 643–658.
[27] A. Janner, T. Janssen, Acta Crystallogr. A 36 (1980) 399–408.
[28] A. Janner, T. Janssen, Acta Crystallogr. A 36 (1980) 408–415.
[29] B.-O. Marinder, J. Solid State Chem. 160 (2001) 62–68.